NANO LETTERS

2008
Vol. 8, No. 3
826-831

Strain Measurements on Individual Single-Walled Carbon Nanotubes in a Polymer Host: Structure-Dependent Spectral Shifts and Load Transfer

Tonya K. Leeuw,[†] Dmitri A. Tsyboulski,[†] Pavel N. Nikolaev,[‡] Sergei M. Bachilo,[†] Sivaram Arepalli,[‡] and R. Bruce Weisman*[,†]

Department of Chemistry, Richard E. Smalley Institute for Nanoscale Science and Technology, and Center for Biological and Environmental Nanotechnology, Rice University, 6100 Main Street, Houston, Texas 77005, and ERC Inc./NASA Johnson Space Center, Mail Stop ES-4, 2101 NASA Parkway, Houston, Texas 77058

Received November 2, 2007; Revised Manuscript Received January 18, 2008

ABSTRACT

The fluorescence spectra of individual semiconducting single-walled carbon nanotubes embedded in polymer films were measured during the application of controlled stretching and compressive strains. Nanotube band gaps were found to shift in systematic patterns that depend on the (*n,m*) structural type and are in excellent agreement with the predictions of theoretical models. Loss of nanotube−host adhesion was revealed by abrupt irregularities in plots of spectral shift vs strain.

Single walled-carbon nanotubes (SWCNTs) are novel artificial nanomaterials with exceptional physical properties that include very high tensile strength.[1] This has made them attractive as strengthening additives for advanced composites in which the nanotubes provide mechanical reinforcement through load transfer from the host matrix.[2,3] The performance of such composites can often be limited by interfacial adhesion between nanotube and matrix.[4] To understand the microscopic processes controlling the macroscopic behavior of a SWCNT composite, it is therefore desirable to study load transfer, strain, and interfacial adhesion limits for individual nanotubes within the composite. In this report, we describe the use of single-nanotube fluorescence spectroscopy to make such in situ measurements on SWCNTs subjected to calibrated external strains while embedded in PMMA.

Our experiments exploit the near-IR band gap photoluminescence of semiconducting SWCNTs. Samples of SWCNTs contain a variety of distinct structural species, each labeled by a pair of integers, (*n*,*m*), defining the diameter and chiral angle. Most nanotube species are semiconducting, and the near-IR emission arises from electron–hole recombination across their band gaps. Because these gaps depend on nanotube physical structure, each species emits light at a characteristic peak wavelength that can be mapped to its (*n*,*m*) identity through an established spectroscopic assignment.[5,6] It has been predicted that axial strain alters the band gaps of SWCNTs in a highly structure-specific pattern.[7] We have used near-IR fluorescence microscopy to detect and structurally identify individual SWCNTs and then to monitor shifts in their emission spectra as they are subjected to calibrated strains through deformations of the surrounding matrix. The resulting strain-induced shifts are determined for a variety of (*n*,*m*) species and compared to quantitative theoretical predictions. These experiments also clearly reveal the abrupt slippage of individual SWCNTs within the matrix through irregularities in spectral shifts as a function of host strain. Our studies thereby provide an incisive probe of load transfer limits at the scale of individual nanoparticles.

In 2000, Yang, et al. used a simple model of SWCNT electronic structure to predict chirality-dependent variations of the semiconducting band gaps under axial strain.[7] Recent experiments have explored this effect through spectroscopic studies of nanotube ensembles and individual SWCNTs. In the ensemble experiments, a change in matrix temperature was typically used to induce strain through differential thermal expansion of the nanotube and the host matrix.[8–11] These studies confirmed characteristic structure-specific patterns of band gap shifts under strain,[8,9] and clarified the smaller changes in band gap related to temperature and

* Corresponding author. E-mail: weisman@rice.edu.
[†] Rice University.
[‡] ERC Inc./NASA Johnson Space Center.

10.1021/nl072861c CCC: $40.75
Published on Web 02/26/2008

hydration.[10,11] However, the strain values in those investigations were not well calibrated. Some other studies have been reported for individual nanotubes deposited on surfaces or suspended in air and then manipulated by atomic force microscopy or micromanipulators.[12–15] Because these methods also suffer from poor strain calibration, they do not permit quantitative tests of the theoretical model predictions. In another type of ensemble measurement, resonance Raman spectra have been studied for SWCNTs in composites. The intensities of radial breathing mode signals changed systematically as strain shifted the nanotube optical transition energies into or out of resonance with laser excitation sources, but SWCNT spectral shifts were not quantified as a function of strain.[16,17]

In our experiments, small quantities of raw HiPco SWCNTs were suspended by ultrasonic agitation in aqueous ~10 mg/mL solutions of sodium dodecylbenzenesulfonate (SDBS), as described earlier.[18] A 100 μL portion of the suspension was mechanically mixed into 5 mL of a viscous solution of poly(methylmethacrylate) (PMMA; 350000 MW) in *o*-xylene. This inhomogeneous mixture was continuously mixed at 70 °C until the water evaporated and the mixture became clear. In this way, SWCNTs with small amounts of SDBS were introduced into the nonpolar medium of PMMA in *o*-xylene. The resulting SWCNT suspension was spin-coated onto a 6 mm thick transparent PMMA bar and became fused to the bar after evaporation of the *o*-xylene. This gave a ~20 μm thick top layer of PMMA containing sparse disaggregated nanotubes. To aid navigation of the sample under the microscope, a 200 mesh TEM finder grid was fixed over the film. Uniaxial compression or extension loads were applied to the top PMMA layer (containing nanotubes) by bending the PMMA bar in either direction using a custom-built four-point bending stage. A bare resistive strain gauge (EA-13-031DE-350, Measurements Group, Inc.) was mounted directly on the top PMMA layer, and the surface strain was measured to an accuracy of $\sim 2 \times 10^{-4}$ with a P-3500 half-bridge strain reader. Because bending strain is distributed linearly through the 6 mm thickness of the bar, strain within the ~20 μm spin-coated top layer can accurately be considered uniform and equal to the strain at its surface.

We measured fluorescence excitation−emission maps of bulk SWCNT samples using a J-Y Spex Fluorolog 3-211 spectrofluorometer equipped with a liquid nitrogen cooled InGaAs detector. Near-IR fluorescence imaging and spectroscopy of individual SWCNTs were performed using a specialized apparatus, described previously,[19] based on an inverted Nikon TE-2000U microscope with an Ealing 36 × 0.5 NA reflective objective. A combination of a dichroic beam splitter and a dielectric 946 nm long-pass filter was used to select emission wavelengths greater than 950 nm. A liquid nitrogen cooled InGaAs camera (Roper Scientific OMA-V 2D) sensitive between 900 and 1600 nm was installed on one microscope output port. Another output port was coupled via fiber optic cable to the input slit of a J-Y C140 spectrograph equipped with a 512 element InGaAs array (OMA-V, Roper Scientific). In this way, near-IR emission spectra could be acquired from a spatial region of ~2.8 × 2.8 μm at the sample. Samples were excited with diode lasers emitting at 658, 730, or 785 nm. The excitation polarization axis was controlled with a crystalline polarizer and an achromatic $\lambda/2$ retardation plate. During the measurements, excitation polarization was adjusted to be parallel to the deformation axis.

According to the model of Yang, et al.,[7] the SWCNT band gap shift ΔE_{ii} depends on the uniaxial strain ε as:

$$\Delta E_{ii} = (-1)^{i+1}(-1)^{k+1} \cdot 3t_0(1+\nu)\cos(3\theta) \cdot \varepsilon \qquad (1)$$

where i equals 1 and 2 for E_{11} and E_{22} transitions, respectively, k is the *mod* index of a nanotube, which equals $mod(n\text{-}m,3)$, t_0 is the electron hopping parameter, ν is the SWCNT Poisson ratio, and θ is the SWCNT chiral angle, which ranges from 0° (zigzag) to 30° (armchair). Equation 1 predicts that spectral shifts of *mod* 1 and *mod* 2 nanotubes occur in opposite directions and that larger shifts are expected for smaller chiral angles. If these characteristic spectral shift patterns are observed for SWCNTs in solid samples, it suggests that axial strain has been induced by interactions with the host matrix.[8]

Our experiments require the (n,m) identities of individual nanotubes to be deduced from their spectral transitions. This is straightforward for SWCNTs in aqueous SDS or SDBS surfactant, for which a well-established assignment precisely links peak positions to (n,m) structures.[5,6] However, the nanotubes in our deformed PMMA films will show shifted spectral transitions that must be remapped to (n,m) structures. Three factors are expected to cause spectral shifts. First, the dielectric environment of PMMA differs from that of SDBS. Second, the dried PMMA film may exert some strain on the embedded SWCNTs even before it is deliberately deformed. Finally, deformation of the film will induce further spectral shifts that are the subject of this study. To find the structure-assigned peak positions of SWCNTs in solid PMMA films before deliberate deformation, we measured excitation–emission maps for bulk nanotube samples (~10 mg/L) in solid PMMA and in a fluid solution of PMMA in *o*-xylene (Figure 1a). Compared with the spectra in SDBS, the broadened peaks in fluid PMMA are systematically red-shifted. They show the same pattern as that in SDBS and are readily remapped to (n,m) structures. Figure 1a illustrates that the peaks in solid PMMA (black circles) are shifted significantly from those in fluid PMMA (white circles). These shifts are plotted in Figure 1b for the E_{11} and E_{22} transitions as a function of the structural factor $(-1)^{k+1}\cos(3\theta)$ from eq 1. The linear variations apparent for both ΔE_{22} and ΔE_{11} (with slopes of 134 ± 15 and −175 ± 24 cm^{-1}) reveal compressive strain induced by stress in the solid dried film. A different effect causes the y-offsets of these linear best fits to differ significantly from zero (−55 ± 10 cm^{-1}), corresponding to a systematic shift to longer transition wavelengths for nanotubes in solid PMMA. We attribute this to the higher dielectric constant of solid PMMA compared to the solution of PMMA in *o*-xylene. The findings described above allowed us to assign (n,m) identities to spectral emission features of SWCNTs in PMMA films before deformation. To confirm the identifications, we also

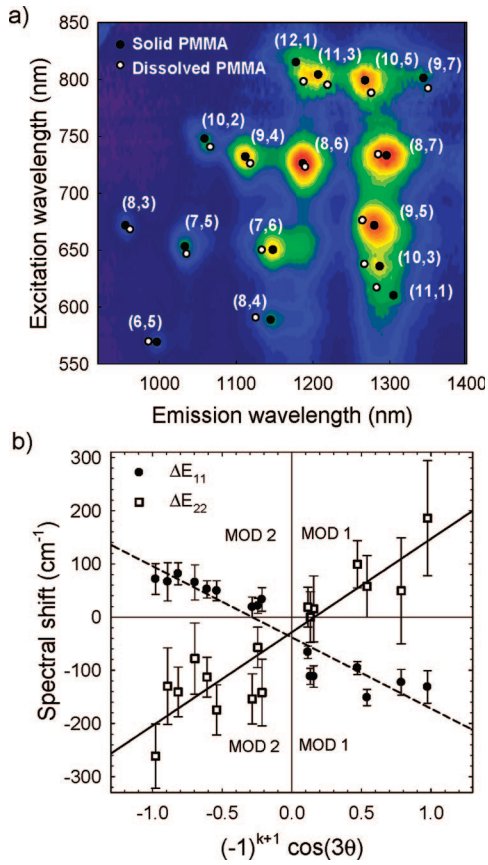

Figure 1. (a) Excitation–emission matrix of SWCNTs in a dried PMMA film. Black circles mark fluorescence maxima of each (*n*,*m*) structure. White circles show positions of the corresponding peaks in liquid PMMA. (b) Shifts in SWCNT E_{22} and E_{11} transition energies between solid and dissolved liquid PMMA media as a function of nanotube structural factor. The lines show linear fits.

excited individual nanotubes with different excitation lasers and checked that the emission intensities (normalized to laser power) displayed a dependence on excitation wavelength consistent with the expected E_{22} peak position.

To measure deformation-induced spectral shifts of individual SWCNTs, we used fluorescence microscopy to image a sparse set of nanotubes in the thin film fused to the PMMA bar on the bending stage. Figure 2a shows a representative image. For each SWCNT, the angle α between its axis and the direction of applied strain was determined to an accuracy better than 5° by recording emission intensities while rotating the polarization plane of the excitation laser (Figure 2b). The high modulation depths seen in these plots indicate that none of the nanotubes observed in our study have significant curvature. The effective applied axial strain, σ, for each SWCNT was then taken to be $\varepsilon_{film} \cos \alpha$, the projection along that nanotube's axis of the uniaxial strain measured in the PMMA film. As incremental extension and compression strains of up to 0.01 were applied to the sample, emission spectra of the individual SWCNTs were recorded at each strain level. These fluorescence spectra were then analyzed by least-squares fitting to Lorentzian functions to determine their peak positions.

We generally found that at small strains (σ below ~0.005), the emission peak maxima of individual SWCNTs shift proportionally to the strain (Figure 3). The direction of spectral shift with strain is determined by the nanotube *mod* index, in agreement with the prediction of eq 1. Examples of this behavior are shown in Figure 4 for (8,7) and (10,2) SWCNTs. Emission from the (8,7) nanotube, a *mod* 1 structure, is shifted to the blue by extension and to the red by compression. This trend is reversed for the (10,2) SWCNTs, which are of *mod* 2 type.

For matrix strain magnitudes exceeding 0.004 to 0.006, we frequently observed deviations from linearity, as seen in Figures 3 and 4. Similar sublinear behavior has been reported for ensemble Raman spectra of SWCNTs embedded in epoxy.[20] This was interpreted as evidence of incomplete load transfer arising from debonding, slipping, or buckling of nanotubes in the deformed polymer. Our data shown in Figure 4b,d for a (10,2) SWCNT are especially revealing. As the polymer film is first loaded in extension, the emission maximum shifts linearly up to $\sigma = 0.004$. The nanotube then apparently slips relative to the PMMA matrix for strains between 0.004 and 0.008 (region A), but recovers to nearly the same slope between 0.008 and 0.01. As the polymer film is then compressed from $\sigma = 0.01$ to $\sigma = -0.008$, it shows two linear regions ($0.002 < \sigma < 0.01$ and $-0.004 < \sigma < -0.002$) and two buckling or slipping regions (regions B and C). The subsequent extension to $\sigma = 0$ is nearly linear. Spectral broadening is often (but not always) observed in

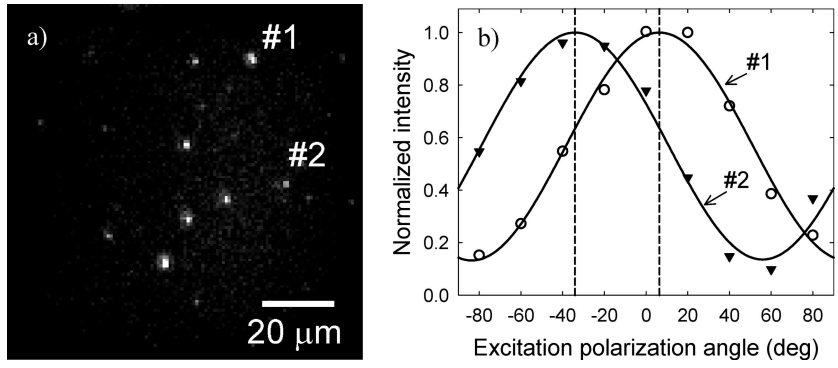

Figure 2. (a) Near-IR fluorescence image of SWCNTs in a PMMA film. (b) Dependence of emission intensities from SWCNT no. 1 and no. 2 on the excitation polarization angle. The angle between nanotube axis and the axis of applied strain equals 5° and −34° for SWCNTs no. 1 and no. 2, respectively.

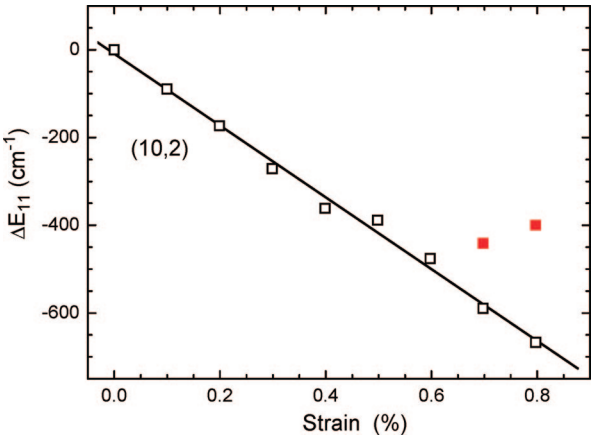

Figure 3. Spectral shift in the emission peak of a (10,2) SWCNT in PMMA as a function of matrix strain. At strains larger than 0.6%, the emission spectrum splits into two components with shifts marked by the open and solid symbols. The solid line is a least-squares fit to the open symbol points.

the regions of nonlinearity, suggesting that strain along the nanotube can be nonuniform.

An example of intriguing behavior is illustrated in Figure 5, which shows the emission spectrum of a (10,2) nanotube splitting into two peaks at $\sigma > 0.006$ when loaded in extension. The bimodal spectrum at $\sigma = 0.008$ was deconvoluted into the two Lorentzian components drawn as dashed lines. When the peak positions are graphed as a function of strain to give a spectral load transfer plot (Figure 3), bifurcation into two components is seen for strains above ~0.006. We suggest that this spectral splitting occurs when a segment of the SWCNT (~1/3, judging from emission intensity) starts slipping near $\sigma = 0.006$ while the rest of the nanotube remains fully attached to the polymer matrix. We find that the deviations from linearity in spectral load transfer plots vary substantially and unpredictably from nanotube to nanotube in our samples. These variations apparently reflect molecular-level differences in the nanotube−matrix interactions and suggest that the load transfer to each nanotube is dominated by relatively few localized sites of strong adhesion.

Despite the observed deviations from linearity, all studied nanotubes also show clear regions of linear load transfer. We have considered only these linear regions to find the average values of slopes $d\Delta E_{11}/d\sigma$ for various nanotube structures. In the examples above, slopes are $(1.3 \pm 0.2) \times 10^4$ cm^{-1} for the (8,7) tube of Figure 4c, $(-8.1 \pm 0.2) \times 10^4$ cm^{-1} for the (10,2) tube of Figure 4d, and $(-7.8 \pm 0.3) \times 10^4$ cm^{-1} for the (10,2) tube of Figures 3 and 5. We determined these values for 14 SWCNTs of 10 different (n,m) species. Figure 6 shows the resulting set of $d\Delta E_{11}/d\sigma$ values plotted as a function of $\cos(3\theta)$, as suggested by the form of eq 1. In agreement with the theoretical model, we find a linear relation represented by the best-fit line, with an intercept of zero and a slope of $(7.1 \pm 0.3 \times 10^4)$ cm^{-1}. This line falls well within the shaded region that was calculated from eq 1 using conventional values for t_0 (2.4−2.9 eV, or ~19000−23000 cm^{-1})[1] and ν (0.15−0.25).[21,22] In the simple electronic structure model

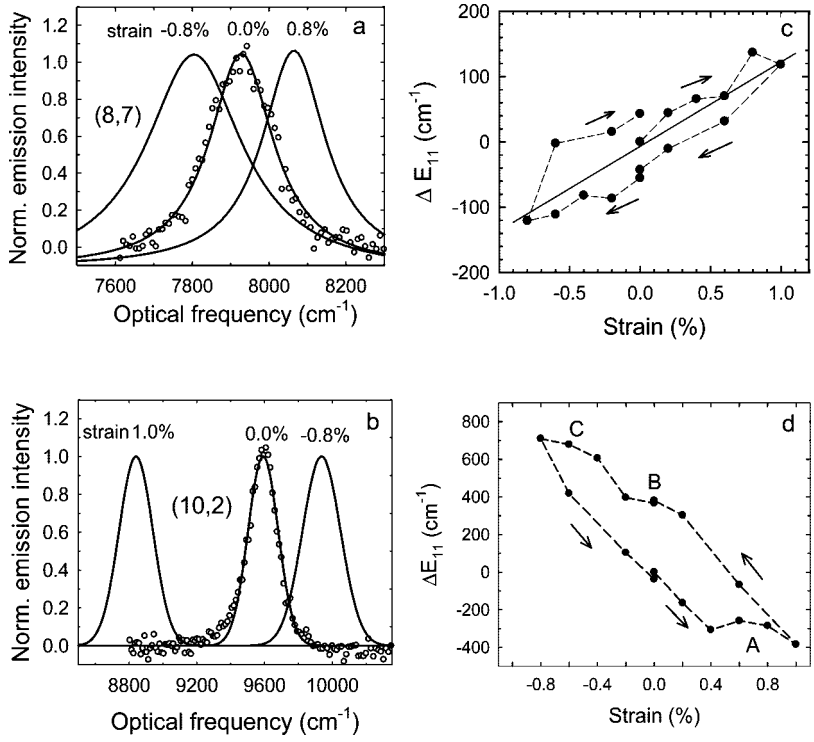

Figure 4. (a,b) Emission spectra of (8,7) and (10,2) SWCNTs in PMMA at different levels of uniaxial matrix strain. SWCNT spectral data were fitted with Lorentzian functions to give the solid curves. For clarity, data points are shown only for the unstrained spectra. (c) The change in SWCNT E_{11} spectral position with matrix strain for the (8,7) nanotube in (a). (d) The change in SWCNT E_{11} spectral position with matrix strain for the (10,2) nanotube in (b). Nanotube slippage is apparent in the regions marked A, B, C. Arrows show the sequence in which the data points were measured.

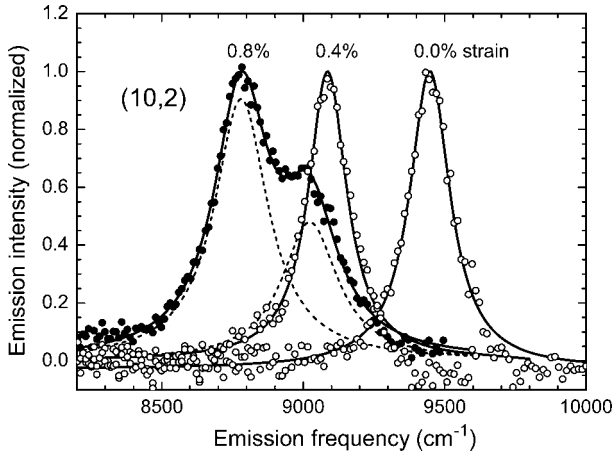

Figure 5. Emission spectra (points) of a (10,2) SWCNT in PMMA at different levels of matrix strain. The data have been fit with Lorentzian profiles, which are drawn as solid curves through the 0.0% and 0.4% points. The 0.8% strain data have been fit with the sum of two Lorentzian components, drawn as dashed curves, which sum to give the solid curve. Spectral peak positions of the two components are plotted in Figure 3.

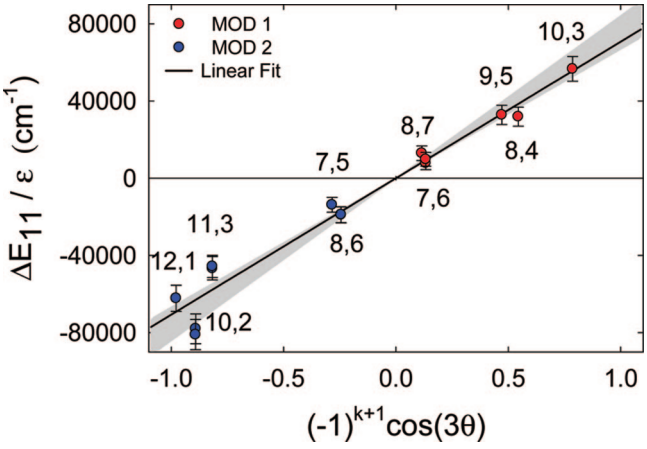

Figure 6. Slopes of experimental strain-induced spectral shifts for different SWCNT species. The solid line is a linear least-squares fit to the data points, and the shaded area shows the range of shifts predicted using the values of t_0 and ν found in the literature.

represented by eq 1, the experimental slope value is much more sensitive to t_0 than to ν. If the typical Poisson ratio ν for the SWCNTs studied here is taken to be 0.15, then our data indicate a t_0 parameter of 2.54 ± 0.15 eV.

It is notable that we observe linear load transfer (i.e., nanotube strain matching matrix strain on the ~3 μm length scale) for maximum strains ranging from 0.002 to 0.008. Some theoretical models of load transfer from a polymer matrix to discontinuous reinforcing fibers predict "shear lag," [23,24] a strain profile along the fiber's length that gradually increases, plateaus, and then decreases. Load transfer in carbon nanotube-reinforced polymers has remained poorly understood, with predictions for the critical length (the scale over which strain increases or decreases in shear-lag models) varying according to the computational approach. Simple estimates based on friction and capillary forces within nanotube bundles suggest critical lengths on the order of 10 μm,[25] whereas molecular dynamics simulations of a nanotube embedded in polyethylene yield a critical length of ~30 μm.[26] We would therefore expect this dimension to be at least a few micrometers, or much greater than the average nanotube length in our samples. This would cause strain within individual nanotubes to vary from zero at the ends to a maximum value in the center that is much smaller than the strain in the surrounding matrix. Such strain profiles would be experimentally manifested in reduced average values of $d\Delta E_{11}/d\sigma$ and in inhomogeneous spectral line broadenings that would appear proportional to matrix strain. However, we find that $d\Delta E_{11}/d\sigma$ values match theory quite well, and no significant line broadening is observed at small strains. This argues against the validity of shear-lag models for this system. An alternative model is that loads are transferred onto nanotubes in our samples via pinning at sites of defects, surface–adsorbates, or other irregularities in the interface that can enhance local adhesion to the matrix. This view is consistent with the observed behavior, especially the peak splitting shown in Figure 4, which suggests the presence of segments within individual nanotubes having different matrix adhesion. Another factor causing such variations in local adhesion, even for pristine nanotubes, may be nonuniformities in the matrix channel surrounding the nanotube that give gaps as well as regions of close contact. SWCNT/matrix contacts may be enhanced by the isotropic compressive strain exerted as solvent evaporates during PMMA film formation and by transverse compression of the matrix (governed by the Poisson ratio) as it is stretched. Finally, taking the Young's modulus of SWCNTs to be ~1 TPa,[27,28] we can estimate the force required to overcome the interfacial adhesion between a typical nanotube and its PMMA matrix as approximately 1.5−6 nN.

In summary, we have monitored the spectroscopic shifts induced by axial strain in individual SWCNTs embedded in a polymer matrix. In the low strain limit, spectral shifts are proportional to strain and show strong dependencies on nanotube chirality and *mod*(*n*-*m*,3) identity that are in good quantitative agreement with theoretical model predictions.

Marked deviations from linearity at higher strains are interpreted as loss of nanotube−host adhesion and apparently reveal slippage of individual nanotubes within the matrix. These effects cannot be observed within polymer composites using other probes of individual nanotubes, and they would be obscured by averaging in ensemble measurements. We believe that near-IR fluorescence spectroscopy will prove a powerful new tool for the development of high performance composite materials by exposing the detailed interactions between nanotubes and their polymer hosts.

Acknowledgment. This work was supported by the Welch Foundation (C-0807), Applied NanoFluorescence, LLC, the NSF Center for Biological and Environmental Nanotechnology (EEC-0647452), and NASA (JSC-NNJ06HC25G). D.A.T. thanks the Welch Foundation for a postdoctoral fellowship (L-C-0004). The authors are also grateful to J. T. Willerson and J. L. Conyers (University

of Texas Health Science Center, Houston) for instrumentation support.

References

(1) Dresselhaus, M. S.; Dresselhaus, G.; Avouris, Ph. *Carbon Nanotubes: Synthesis, Structure, Properties, and Applications*; Springer-Verlag: New York, 2001; Vol. 80.
(2) Ajayan, P. M.; Schadler, L. S.; Giannaris, C.; Rubio, A. *Adv. Mater.* **2000**, *12*, 750–753.
(3) Zhan, G.-D.; Kuntz, J. D.; Wan, J.; Mukherjee, A. K. *Nat. Mater.* **2003**, *2*, 38–42.
(4) Hadjiev, V. G.; Iliev, M. N.; Arepalli, S.; Nikolaev, P.; Files, B. S. *Appl. Phys. Lett.* **2001**, *78*, 3193–3195.
(5) Bachilo, S. M.; Strano, M. S.; Kittrell, C.; Hauge, R. H.; Smalley, R. E.; Weisman, R. B. *Science* **2002**, *298*, 2361–2366.
(6) Weisman, R. B.; Bachilo, S. M. *Nano Lett.* **2003**, *3*, 1235–1238.
(7) Yang, L.; Han, J. *Phys. Rev. Lett.* **2000**, *85*, 154–157.
(8) Arnold, K.; Lebedkin, S.; Kiowski, O.; Hennrich, F. H.; Kappes, M. M. *Nano Lett.* **2004**, *4*, 2349–2354.
(9) Li, L.-J.; Nicholas, R. J.; Deacon, R. S.; Shields, P. A. *Phys. Rev. Lett.* **2004**, *93*, 156104-1–156104-4.
(10) Karaiskaj, D.; Engtrakul, C.; McDonald, T.; Heben, M. J.; Mascarenhas, A. *Phys. Rev. Lett.* **2006**, *96*, 106805-1–106805-4.
(11) Li, L.-J.; Nicholas, R. J.; Chen, C.-Y.; Darton, R. C.; Baker, S. C. *Nanotechnology* **2005**, *16*, S202–S205.
(12) Cao, J.; Wang, Q.; Dai, H. *Phys. Rev. Lett.* **2003**, *90*, 157601-1–157601-4.
(13) Minot, E. D.; Yaish, Y.; Sazonova, V.; Park, J.-Y.; Brink, M.; McEuen, P. L. *Phys. Rev. Lett.* **2003**, *90*, 156401-1–156401-4.
(14) Maune, H.; Bockrath, M. *Appl. Phys. Lett.* **2006**, *89*, 173131-1–173131-3.
(15) Maki, H.; Sato, T.; Ishibashi, K. *Nano Lett.* **2007**, *7*, 890–895.
(16) Lucas, M.; Young, R. J. *Phys. Rev. B* **2004**, *69*, 085405-1–085405-9.
(17) Lucas, M.; Young, R. J. *Compos. Sci. Technol.* **2007**, *67*, 2135–2149.
(18) O'Connell, M.; Bachilo, S. M.; Huffman, C. B.; Moore, V.; Strano, M. S.; Haroz, E.; Rialon, K.; Boul, P. J.; Noon, W. H.; Kittrell, C.; Ma, J.; Hauge, R. H.; Weisman, R. B.; Smalley, R. E. *Science* **2002**, *297*, 593–596.
(19) Tsyboulski, D. A.; Bachilo, S. M.; Weisman, R. B. *Nano Lett.* **2005**, *5*, 975–979.
(20) Hadjiev, V. G.; Lagoudas, D. C.; Oh, E. S.; Thakre, P.; Davis, D.; Files, B. S.; Yowell, L.; Arepalli, S.; Bahr, J. L.; Tour, J. M. *Compos. Sci. Technol.* **2006**, *66*, 128–136.
(21) Kudin, K.; Scuseria, G. E.; Yakobson, B. I. *Phys. Rev. B* **2001**, *64*, 235406-1–235406-10.
(22) Lawler, G. E.; Mintmire, J. W.; White, C. T. *Phys. Rev. B* **2006**, *74*, 125415-1–125415-5.
(23) Cox, H. L. *Br. J. Appl. Phys.* **1952**, *3*, 72–79.
(24) Haque, A.; Ramasetty, A. *Compos. Struct.* **2005**, *71*, 68–77.
(25) Yakobson, B. I.; Samsonidze, G.; Samsonidze, G. G. *Carbon* **2000**, *38*, 1675–1680.
(26) Frankland, S. J. V.; Caglar, A.; Brenner, D. W.; Griebel, M. *J. Phys. Chem. B* **2002**, *106*, 3046–3048.
(27) Lu, J. P. *Phys. Rev. Lett.* **1997**, *79*, 1297-1–1297-4.
(28) Yu, M. F.; Files, B. S.; Arepalli, S.; Ruoff, R. S. *Phys. Rev. Lett.* **2000**, *84*, 5552-1–5552-4.

NL072861C